Journal of Alloys and Compounds 509 (2011) 7116–7120

Contents lists available at ScienceDirect

Journal of Alloys and Compounds

journal homepage: www.elsevier.com/locate/jallcom

Liquid phase separation of Cu–Cr alloys during the vacuum breakdown

Xin Wei, Jiping Wang, Zhimao Yang, Zhanbo Sun*, Demei Yu, Xiaoping Song, Bingjun Ding, Sen Yang

MOE Key Laboratory for Non-equilibrium Synthesis and Modulation of Condensed Matter, State Key Laboratory for Mechanical Behavior of Materials, Xi'an Jiaotong University, Xi'an 710049, PR China

ARTICLE INFO

Article history:
Received 14 February 2011
Received in revised form 27 March 2011
Accepted 2 April 2011
Available online 8 April 2011

Keywords:
Cu–Cr alloys
Vacuum breakdown
Microstructure evolution
Liquid phase separation

ABSTRACT

The microstructures of the surfaces and cross sections of Cu–Cr contact alloys were analyzed after the vacuum breakdown was repeated for 100 times. The results reveal that the liquid phase separation was involved in the microstructure evolution of the alloys during the breakdown. The Cr-rich phase from the liquid separation featured the morphology of spherical- and sheeted-shaped particles. The sizes of the Cr spheres ranged from several nanometers to hundreds of nanometers, and were not strongly dependent on the compositions of the alloys. The large Cr-rich droplets could be elongated and swirled due to the liquid flow, resulting in the formation of the Cr phase with sheeted-shaped particles. The fractions of Cr sheets increased with the increasing of the Cr contents; however, their sizes decreased significantly, compared with those of their parent alloys.

1. Introduction

Cu–Cr alloys with high Cr contents have been widely used in medium-voltage and high-current vacuum interrupters due to their high mechanical strength and good electrical conductivity [1,2]. Various preparation processes have been adopted to produce the Cu–Cr contact alloys, such as vacuum induction melting [3], powder sintering [4], self-consume electrode [5] and arcing melt [6]. It has been found that the properties of the Cu–Cr contact alloys are strongly dependent on their compositions and microstructures, including the grain size, distribution and morphology of Cr phase [3,7]. The refinement of the Cr grains can also improve the properties of the Cu–Cr contact alloys [7–9].

During the switching operation, a vacuum arc is generated in the vacuum interrupter and the Cu–Cr contact alloy is heated by plasma; then a surface melt layer is formed and the original microstructure of the surface layer is evolved [3,4,10–14]. As a result, the dielectric strength of the contact is enhanced after a certain period of the breakdown. Therefore, the first dozens of the breakdown are defined as the conditioning process [3,4]. The above findings indicate that the microstructure evolution of the surface layer will occur during the contact breakdown and that the evolved microstructure plays an important role in the contact alloy performance. However, the mechanism underlying the evolution of the surface microstructure has not been studied in detail.

In the present work, the microstructures of the melt layers after the breakdown of $Cu_{100-X}Cr_X$ alloys (X = 25, 30, 40, 50 in wt%) were analyzed to reveal the mechanism of microstructure evolution during the breakdown. The results indicate that a liquid phase separation is involved in the microstructure evolution of the Cu–Cr contact alloys.

2. Experimental

$Cu_{100-X}Cr_X$ alloys (X = 25, 30, 40, 50 in wt%), which are widely applied as contacts in industry, were used in this experiment. The production process of these contact alloys has been described in details in reference [3]. The samples to be analyzed were cut from the contact alloys and machined to a size of 20mm × 20mm × 5 mm.

The samples were polished mechanically and put into a vacuum chamber. A direct current (DC) voltage of 8 kV was applied between a cathode and an anode in the breakdown experiment. According to our previous studies [3,4,10], a discharge current of 28 A was adopted. The adopted current density was close to that served by Cu–Cr contact alloys under the real conditions. Pure tungsten of Φ0.5 mm was used as the anode and the test sample served as the cathode. The cathode was driven by a step motor upwards to the anode at a velocity of 0.2 mm per minute until the breakdown took place. The breakdown was repeated for 100 times.

The microstructures of the Cu–Cr contact alloys and their breakdown samples were examined using a JSM-7000F scanning electron microscopy (SEM) equipped with an energy dispersion spectrometer (EDS) and a backscattered electron detector. Some breakdown samples were etched in a 35 vol% HNO_3 solution and cleaned by an absolute alcohol for clear observation of the Cr-rich phase.

3. Results

The backscattered electron images of the $Cu_{75}Cr_{25}$ and $Cu_{60}Cr_{40}$ contact alloys are shown in Fig. 1, where the matrix is Cu and the undergrown dendrites are Cr. Coarser dendrites and higher volume fraction of Cr are observed with the increasing of the Cr content in

* Corresponding author. Tel.: +86 29 8266 5892; fax: +86 29 8266 5995.
E-mail addresses: szb@mail.xjtu.edu.cn, xin.wei@stu.xjtu.edu.cn (Z. Sun).

0925-8388/$ – see front matter © 2011 Elsevier B.V. All rights reserved.
doi:10.1016/j.jallcom.2011.04.017

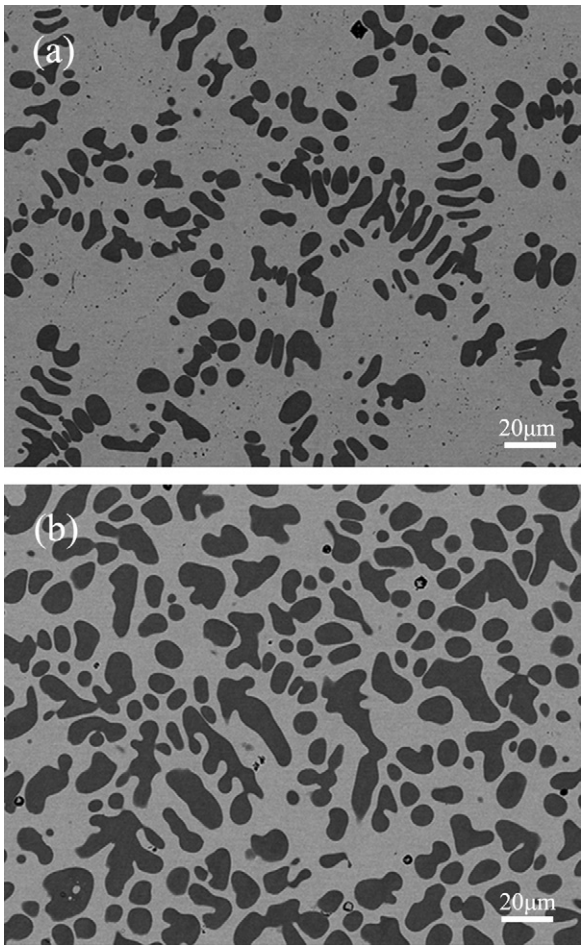

Fig. 1. Microstructures of $Cu_{75}Cr_{25}$ (a) and $Cu_{60}Cr_{40}$ (b) (backscattered electron images).

the alloy. These microstructures are similar to those reported in references [3] and [15].

Fig. 2 shows the surface morphology of the $Cu_{60}Cr_{40}$ contact alloy after the vacuum breakdowns. The morphological patterns observed in the breakdown experiments are called cathode spots [16,17]. Two types of cathode spots are observed: the large pits of conchoidal shape, as denoted by arrow A; and the small irregular pits, indicated by arrow B (Fig. 2(a)). The morphology is similar to that described in reference [18]. The backscattered electron image indicates that the large conchoidal-shaped spots consist of a bright matrix with dark spherical particles (marked by arrow C) and dark regions with irregular shapes (marked by arrow D) (Fig. 2(b)). The dark regions have stamps of flows of the melt alloy with a large number of spheres distributed among the flows. However, in the small irregular pits only a large number of small darker spherical particles are observed (Fig. 2(c)).

Fig. 3 shows the secondary electron images of the etched surface of the $Cu_{60}Cr_{40}$ contact alloy after the breakdowns. Large quantities of spherical and sheeted particles, as shown in Fig. 3(a), are clearly displayed in the region of the large conchoidal-shaped spots after the $Cu_{60}Cr_{40}$ contact alloy was etched. EDS analysis shows that the compositions of the spherical and sheeted particles are similar to that of $Cr_{88}Cu_{12}$. They are called Cr-rich spheres and Cr-rich sheets in the present experiment, respectively. Therefore, the dark spheres, as shown in Fig. 2(b), are Cr-rich spheres, and the dark regions with sheeted shapes are Cr-rich sheets. A large number of spheres but an extremely small number of sheets are observed in the region of the small etched breakdown spots (Fig. 3(b)). The

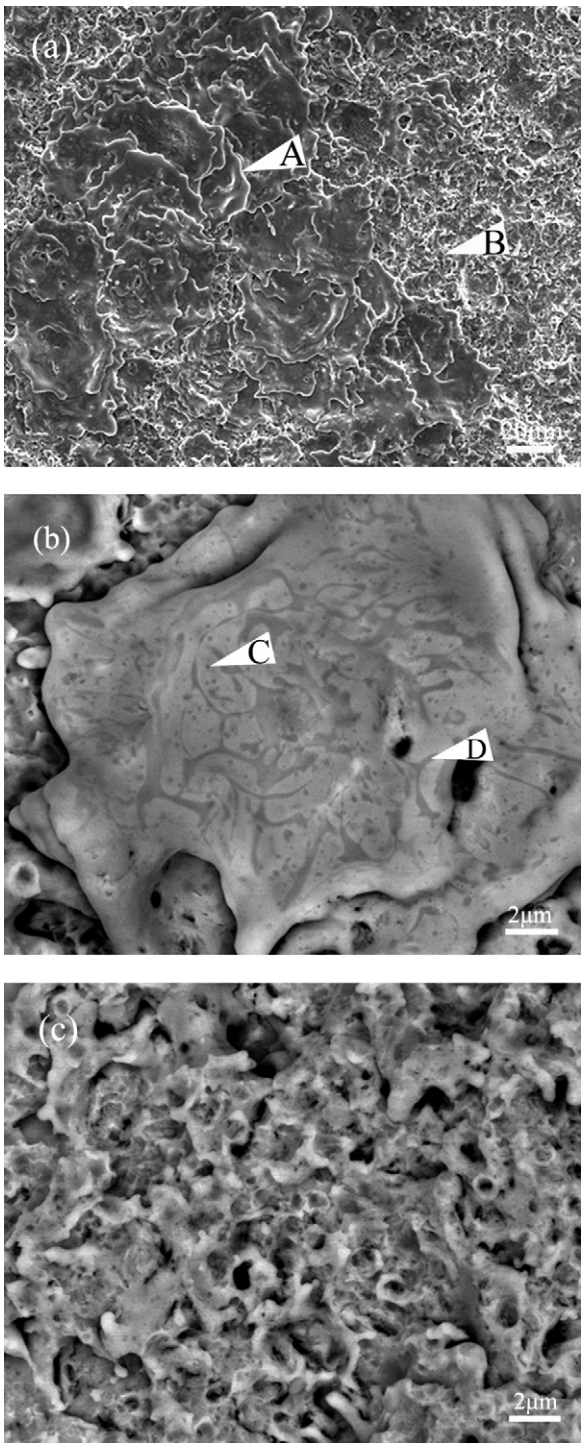

Fig. 2. Morphology and microstructure of $Cu_{60}Cr_{40}$ alloy after breakdowns. (a) Secondary electron image; (b) and (c) backscattered electron images. (Arrow A points to a conchoidal-shaped spot, arrow B points to a small irregular spot, arrow C points to a dark spherical particle and arrow D points to a dark region with irregular shape).

sizes of the Cr-rich spheres vary from only several nanometers to over 400 nm. It can be easily observed that small spheroids can be coagulated to form larger ones, as denoted by arrow A. The above results, in combination with the microstructures of deep supercooled and melt-spun metastable Cu–Co [19–26], Cu–Fe [23,27] and Cu–Cr [28–31] alloys, show that a liquid phase separation is involved in the microstructure evolution. The Cr-rich phase in the breakdown $Cu_{60}Cr_{40}$ alloy, therefore, results from the liquid phase separation.

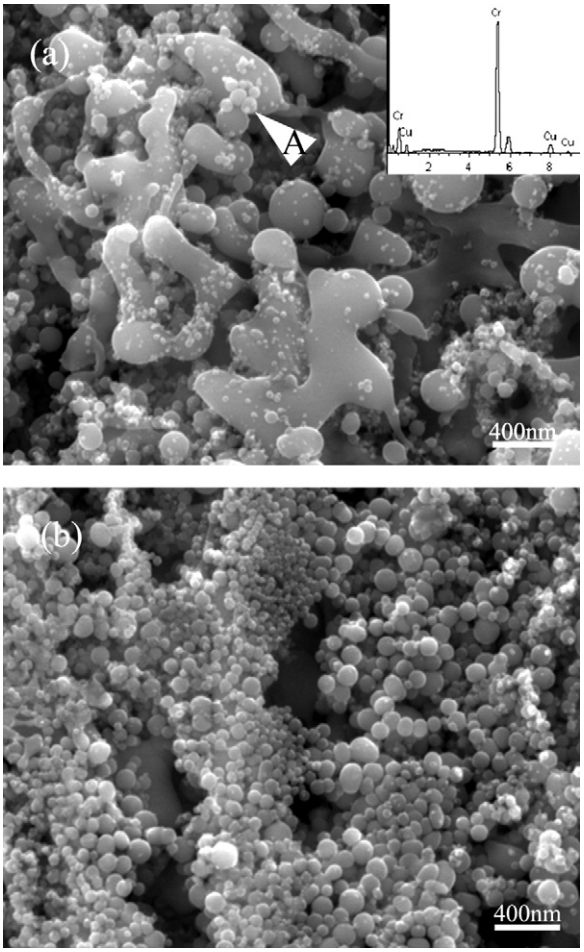

Fig. 3. Morphology of the etched surface of the $Cu_{60}Cr_{40}$ alloy after breakdowns (second electron images), arrow A denoted that small spheroids can be coagulated to form larger ones.

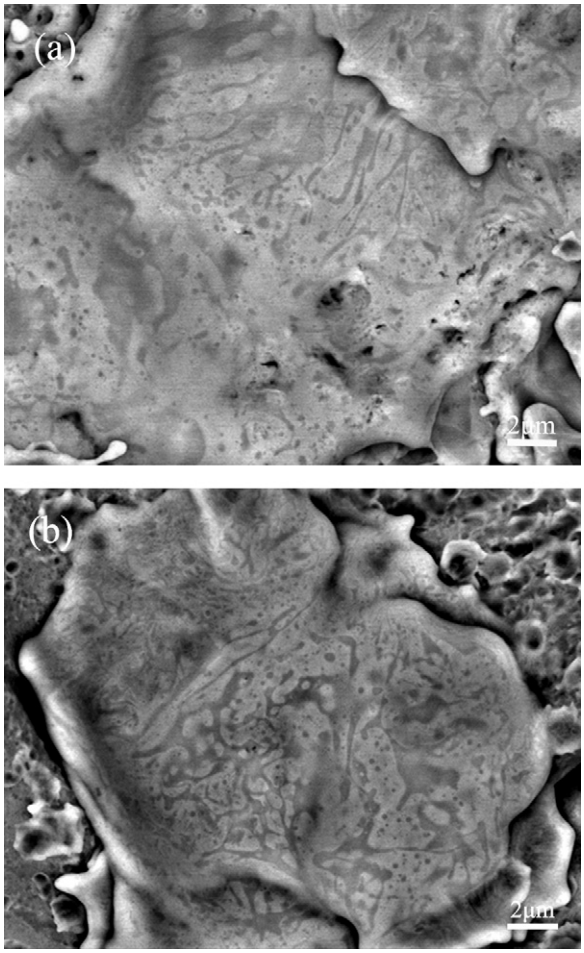

Fig. 4. Microstructures of conchoidal-shaped spots in $Cu_{70}Cr_{25}$ (a) and $Cu_{50}Cr_{50}$ (b) alloys after breakdowns (backscattered electron images).

Fig. 4 shows the backscatter electron images of the large conchoidal-shaped spots in the Cu–Cr alloys with different Cr contents after the breakdowns. Generally, the microstructures consist of Cu-rich matrix, small Cr spheres and Cr sheets with elongated and swirled patterns. The sizes of the Cr spheres are not strongly dependent on the compositions of the Cu–Cr alloys. However, the fraction of the Cr-rich sheets increases with the Cr content and they exhibit varied morphologies.

Fig. 5 illustrates the microstructures of the cross section of the $Cu_{50}Cr_{50}$ melt layer after the breakdowns. The microstructure of the melt layer is significantly different from that of the parent alloy (Fig. 1). Cr-rich spheres and sheets are observed again. The Cr phase in the $Cu_{50}Cr_{50}$ alloy, as shown in Fig. 5(a), melted partially. An interface between the melted and un-melted layers can be seen. The depth of the melt layer is less than 7 μm. A portion of the Cr particles from the liquid phase separation have a tendency to congregate with un-melted Cr-rich dendrites (Fig. 5(b)).

4. Discussion

The Cu–Cr system, similar to the Cu–Co [19–26] and Cu–Fe [23,27] systems, is a liquid metastable binary system with a large positive heat of mixing. Zeng et al. [32] obtained a liquid metastable miscibility gap (MG) by thermodynamic calculation. Jacob et al. [33] revised the MG by a measurement of the activity of Cr in the Cu–Cr liquid. The Cu–Cr binary phase diagram with the metastable miscibility gap is shown in Fig. 6, where the dash lines indicate the MG (binodal lines) and liquid spinodal lines, respectively. When the Cu–Cr melt is cooled below a certain temperature, the liquid will enter the MG zone and be separated into Cu-rich liquid (L1) and Cr-rich liquid (L2), and the liquid phase separation will occur [30]. Our previous studies have experimentally confirmed that the liquid phase separation will occur in the Cu–Cr liquid during the rapid solidification process.

Fig. 7 shows a schematic illustration of the breakdown of a Cu–Cr contact sample and a typical discharge curve measured in this experiment. When the electrodes are within a certain distance from each other, a vacuum breakdown occurs and an arc appears. The contact surface is melted by plasma and a molten pool is formed. The discharge current will disappear suddenly as the current decreases to a certain value, resulting in a chopping. During this process, the current carried by the plasma will decrease gradually with the consumption of the power in the capacitor. Generally, the sustained duration is extremely short although it is dependent on the alloy type and experimental conditions. This means that the melt will cool down and solidify in a moment because the contact body is cold and has large heat conduction ability. A large supercooling will form and the liquid phase separation occurs inevitably according to our previous work [29,30]. The spherical Cr-rich droplets appear and accumulate into larger ones. The Cr spheres, as shown in Fig. 3, are formed after the melt layer is solidified.

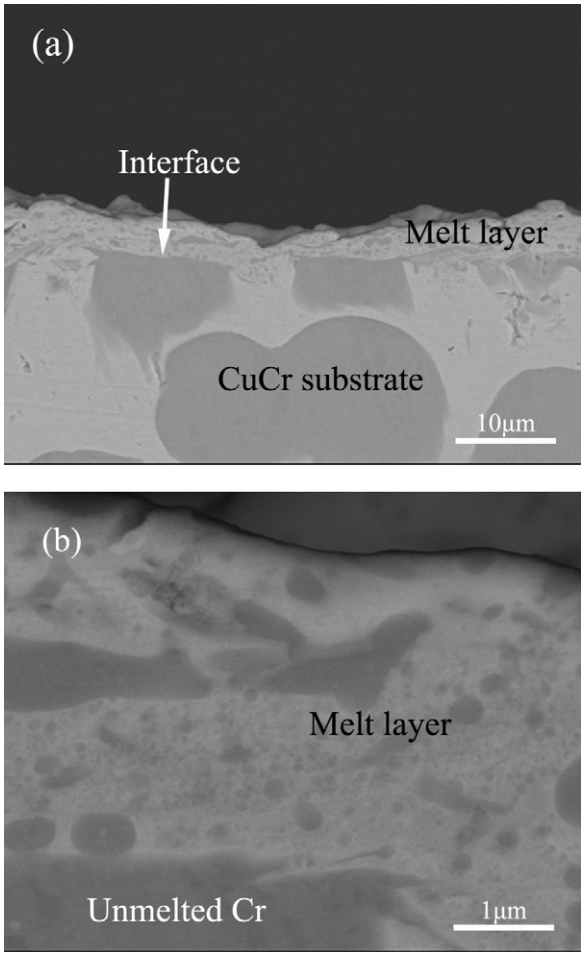

Fig. 5. Microstructure of the cross section of $Cu_{50}Cr_{50}$ alloy after breakdowns. (a) Overall view; (b) up to the interface (backscattered electron images).

Generally, the process of the liquid phase separation can be divided into several stages: formation of droplets, growth and accumulation of the droplets, second liquid phase separation, and solidification of the droplets according to published studies [19–23,34]. Rapid cooling plays an essential role in the formation of a large supercooling. The lower cooling rate will result in larger droplets after liquid phase separation and the size of the droplet decreases with the increasing of the cooing rate [19,29,30]. The growth and accumulation of the droplets have been observed clearly in Fig. 3(a). Fig. 7(b) indicates that the current will decrease gradually within 1.25 ms for the $Cu_{60}Cr_{40}$ alloy. Although the duration is extremely short, the plasma will heat the melt continuously. However, the heating ability of the plasma decreases with the reduction of the current. This will result in a lower cooling rate, which provides an opportunity for Cr-rich droplets to accumulate and grow [19]. More importantly, as the current is reduced, the sizes of the cathode craters will decrease and the melt will not be heated uniformly by the plasma, which will cause a flow of the melt. The grown Cr-rich droplets will be elongated and swirled because the liquid phase separation occurs before the solidification of the alloy (Figs. 3 and 4). Because the flow only appears on the sample surface, the sheets have been used to describe the Cr phase.

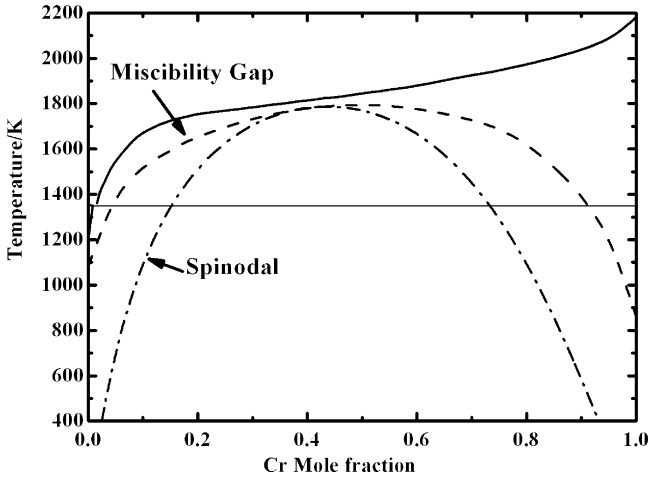

Fig. 6. Cu–Cr binary phase diagram with metastable liquid miscibility gap [33].

Another reason for the formation of the Cr sheets is that a spraying, as shown in Fig. 7(a), occurs. The cooling rate of the alloy droplets is smaller than that of the melts in the pool; the liquid phase separation and the liquid flow proceed simultaneously. Small Cr-rich droplets form continuously and some extremely fine Cr particles always appear during the liquid phase separation process, which is in accordance with previously reported results [19,29]. Cr sheets will not occur in large quantities in the small breakdown spots due to the high cooling rate and limited melt flow.

The supercooling for the liquid phase separation decreases with the increase in the Cr content when the Cr content is less than 50% (Fig. 6). The more completely the liquid phase separation proceeds, the larger Cr sheets will occur. In this study, the cooling rate during the breakdown is extremely high and the supercooling is extremely large due to the small thickness of the melt layer. As a result, all the Cu–Cr melts in the composition range enter the MG zone. It may be concluded that the composition of the Cu–Cr alloy has slight effect on the liquid phase separation.

The real contacts used in switches have slightly different performance from those in this experiment. When the real switches are turned on, arc appears and the contact surface is melted by plasmas, resulting in a molten pool. The depth of the molten pool increases with the reduction of the distance between the electrodes. The arc will extinguish after the electrodes contact each other. The alloy melt is cooled down and solidified. When the switches are turned off, the arc appears as the electrodes are separated. The molten pool forms again. As the electrodes depart to a certain distance, the arc extinguishes and the melts are cooled and solidified rapidly. Therefore, the off-action of the real switches is similar to that in this experiment. In real situations, the liquid phase separation will occur inevitably when the switches are turned on and off alternately. The liquid phase separation process will have a substantial effect on the property and service life of an interrupter. The liquid phase separation which occurs when the switch is turned off has a more important effect on the contact property because it influences the breakdown and arc erosion rate when the electrodes initiate the next breakdown.

The Cr phase in the melt layer is much smaller than the primary Cr dendrites in the alloy (Fig. 5). This refinement can remarkably improve the dielectric strength according to previously reported findings [7–9]. The appearance of Cr-rich particles with the spherical shape is beneficial to the improvement of the dielectric strength of the Cu–Cr contact materials. However, the large size of Cr sheets with an irregular shape is harmful to the performance of the Cu–Cr contact materials. Further studies are needed to control and refine the Cr sheets in the surface layer.

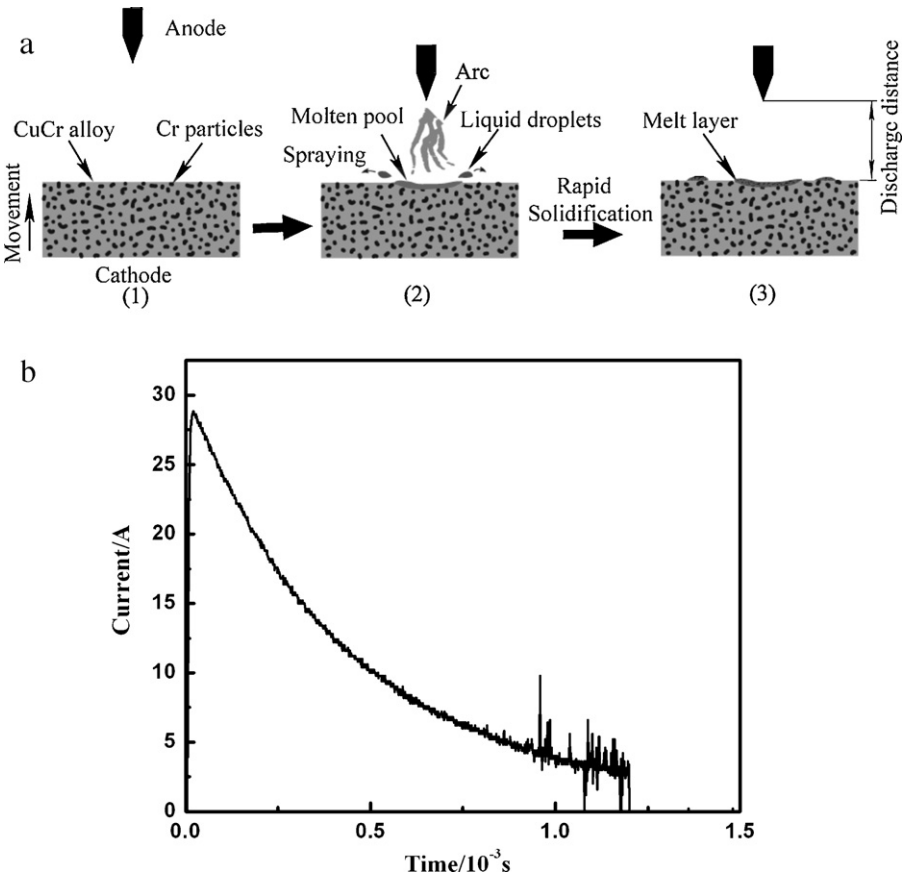

Fig. 7. Schematic illustration of vacuum breakdown process (a) and discharge curve (b) for $Cu_{60}Cr_{40}$ alloy.

5. Conclusions

It has been confirmed that liquid phase separation is involved in the microstructure evolution of Cu–Cr alloys during the repeated vacuum breakdowns. The Cr phase with the morphology of spheres and sheets appears in the melt layer. The size of the Cr spheres from the liquid phase separation exhibits a wide range and is not strongly dependent on the parent composition. The fractions of Cr sheets increase obviously with the increasing of the Cr contents. The formation of the microstructures with different morphologies is dependent on the liquid flow pattern during the liquid phase separation.

Acknowledgement

This research is supported by the National Science Foundation of China (50834003, 50871081) and the National High Technology Research and Development Program of China (863 program: 2007AA03Z512).

References

[1] P.G. Slade, IEEE Trans. CPMT 17 (1994) 96–106.
[2] W.P. Li, Proc. 19th ISDEIV, 2000, pp. 380–383.
[3] C.Y. Zhang, Y.P. Wang, Z.M. Yang, Y. Guo, B.J. Ding, J. Alloys Compd. 366 (2004) 289–292.
[4] B.J. Ding, Z.M. Yang, X.T. Wang, IEEE Trans. CPMT 19 (1996) 76–81.
[5] S.X. Xiu, J.Y. Zou, J.J. He, High-Votage Electr. Equip. 36 (2000) 40–43.
[6] F. Zhao, Z.M. Yang, B.J. Ding, Trans. Nonferrous Met. Soc. China 10 (2000) 73–75.
[7] W.F. Rieder, M. Schussk, W. Glatzle, E. Kny, IEEE Trans. CPMT 12 (1989) 273–283.
[8] Y.P. Wang, B.J. Ding, IEEE Trans. CPMT 22 (1999) 467–472.
[9] R. Muller, Simens Forsch. Entwicklungsber 17 (1988) 105–111.
[10] Z.M. Yang, Q. Yan, B.J. Ding, X.T. Wang, Proc. 41th IEEE Holm Conf. on Electr. Contacts, 1995, pp. 242–246.
[11] B. Gellert, E. Schade, E. Dullni, IEEE Trans. Plasma Sci. 15 (1987) 545–551.
[12] B. Gellert, E. Schade, Proc. 14th ISDEIV, vol. 1, 1990, pp. 450–454.
[13] P. Frey, N. Klink, R. Michal, K.E. Saeger, IEEE Trans. Plasma Sci. 17 (1989) 734–740.
[14] S.X. Xiu, S.L. Jia, J.M. Wang, Proc. 20th ISDEIV, 2002, pp. 523–525.
[15] C.Y. Zhang, Z.M. Yang, Y.P. Wang, B.J. Ding, Y. Guo, J. Mater. Process. Technol. 178 (2006) 283–286.
[16] Y.F. Su, W.G. Chen, F.Z. Wang, B.J. Ding, Mater. Lett. 59 (2005) 1046–1049.
[17] C.Y. Zhang, Z.M. Yang, Y.P. Wang, B.J. Ding, Phys. Lett. A 318 (2003) 435–439.
[18] Z.M. Yang, Q.L. Zhang, C.Y. Zhang, Y. Sun, B.J. Ding, Phys. Lett. A 353 (2006) 98–100.
[19] Z.B. Sun, X.P. Song, Z.D. Hu, S. Yang, G.Y. Liang, J. Sun, J. Alloys Compd. 319 (2001) 266–270.
[20] A. Munitz, R. Abbaschian, J. Mater. Sci. 26 (1991) 6458–6466.
[21] X.P. Song, S.W. Mahon, R.F. Cochrane, B.J. Hickey, M.A. Howson, Mater. Lett. 31 (1997) 261–266.
[22] M.B. Robinson, D. Li, T.J. Rathz, G. Willims, J. Mater. Sci. 34 (1999) 3747–3753.
[23] S.P. Elder, A. Munitz, G.J. Abbaschian, Mater. Sci. Forum 50 (1989) 137–150.
[24] C.D. Cao, T. Letzig, G.P. Görler, D.M. Herlach, J. Alloys Compd. 325 (2001) 113–117.
[25] C.D. Cao, G.P. Görler, D.M. Herlach, B. Wei, Mater. Sci. Eng. A 325 (2002) 503–510.
[26] T. Nagase, Y. Umakoshi, J. Alloys Compd. 505 (2010) L43–L46.
[27] T. Nagase, A. Yokoyama, Y. Umakoshi, J. Alloys Compd. 494 (2010) 295–300.
[28] Z.B. Sun, C.Y. Zhang, Y.M. Zhu, Z.M. Yang, B.J. Ding, X.P. Song, J. Alloys Compd. 361 (2003) 165–168.
[29] Z.B. Sun, Y.H. Wang, J. Guo, Y.M. Zhu, X.P. Song, R.H. Zhu, Mater. Sci. Eng. A 452–453 (2007) 411–416.
[30] Z.B. Sun, Y.H. Wang, J. Guo, Trans. Nonferrous Met. Soc. China 16 (2006) 998–1002.
[31] Z.M. Zhou, Y.P. Wang, J. Gao, M. Kolbe, Mater. Sci. Eng. A 398 (2005) 318–322.
[32] K.J. Zeng, M. Hämäläinen, J. Alloys Compd. 220 (1995) 53–61.
[33] K.T. Jacob, S. Priya, Y. Waseda, Z. Metallkd. 91 (2000) 594–600.
[34] C.D. Cao, D.M. Herlach, M. Kolbe, G.P. Görler, B. Wei, Scr. Mater. 48 (2003) 5–9.